Supporting Information

Effect of indium–doping of γ–alumina on the stabilization of PtSn alloyed clusters prepared by surface organostannic chemistry

Ali Nazir Jahel [a,b], Virginie Moizan-Baslé [a], Céline Chizallet [a], Pascal Raybaud [a], Josette Olivier-Fourcade [b], Jean-Claude Jumas [b], Priscilla Avenier [a], Sylvie Lacombe [a*]

[a] IFP Energies nouvelles, Rond-point de l'échangeur de Solaize B.P. 3, 69360 Solaize (France).

[b] ICG/AIME (UMR 5253 CNRS), Université Montpellier II CC 15-02, Place E. Bataillon, 34095 Montpellier Cedex 5 (France).

1. Selected STEM pictures of reduced catalysts

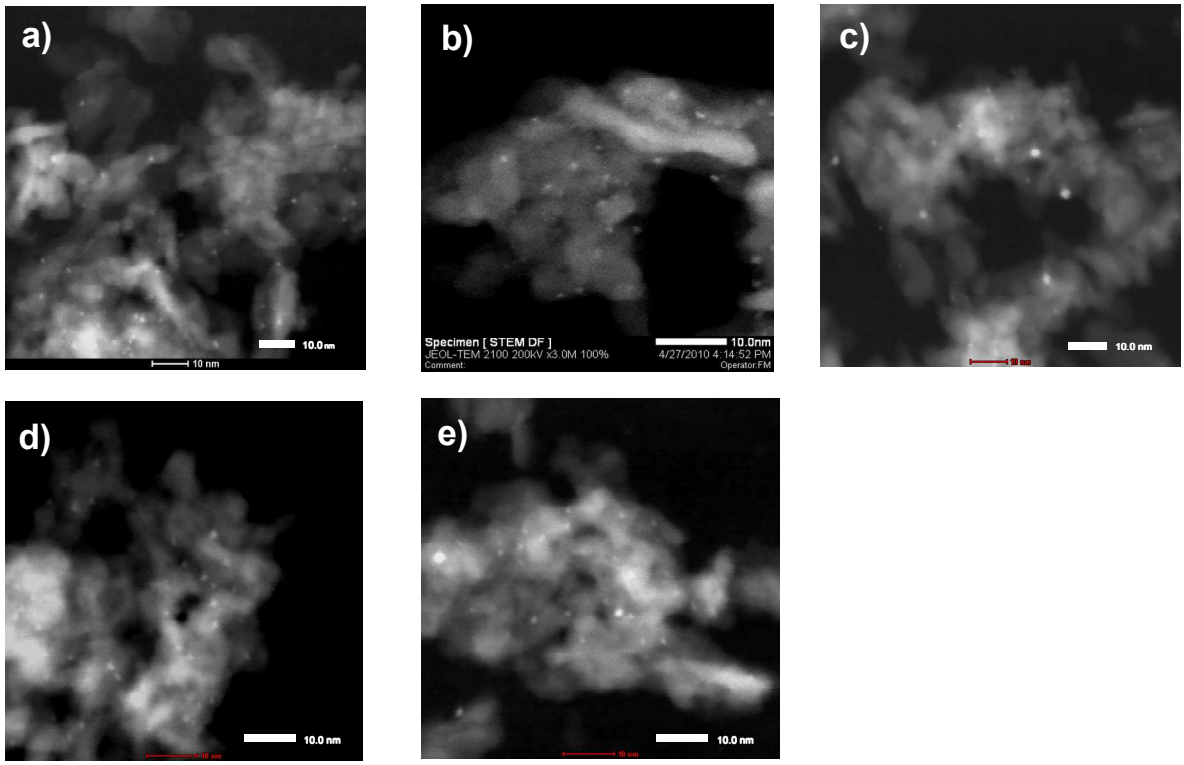

Figure S1. Selected STEM pictures of reduced catalysts: a) Pt/Al_2O_3In-Cl, b) $PtIn/Al_2O_3$-Cl, c) $SnPt/Al_2O_3$-Cl, d) $SnPtIn(0.38)/Al_2O_3$-Cl and e) $SnPt/Al_2O_3In(0.38)$Cl.

2. Local platinum characterisation: Pt L_3-edge XANES on reference platinum catalysts

Fig. S2 shows a comparison of the XANES spectra at the Pt L_3 edge of a reduced Pt/Al_2O_3-Cl catalyst with two reference samples: Pt metal foil (Pt^0 oxidation state) and PtO_2/Al_2O_3-Cl (Pt^{+4} oxidation state). When exciting the Pt L_3 edge, empty 5d electronic states are probed and the intensity of the whiteline is a direct measure of the number of holes in the band.[i,ii,iii,iv,v,vi,vii]

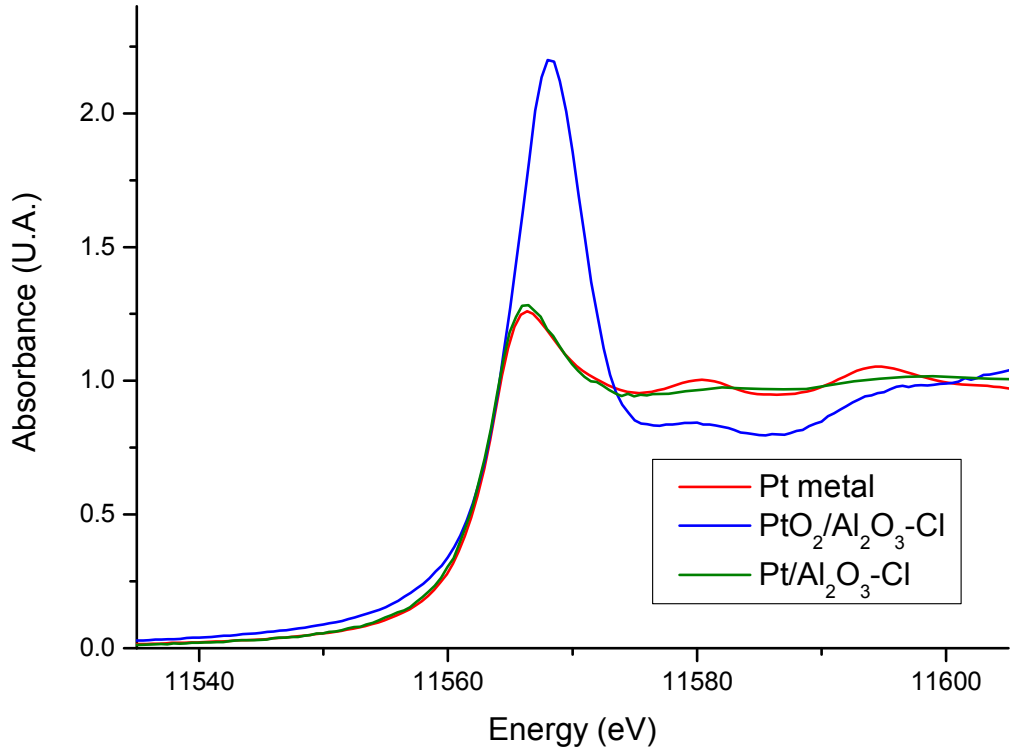

Figure S2. XANES spectra at the Pt L_3-edge of Pt metal, PtO_2/Al_2O_3-Cl and reduced Pt/Al_2O_3-Cl.

In the metallic state (Pt metal) the whiteline shows a maximum absorption intensity around 11566 eV which is not very intense and shifted in energy compared with the absorption intensity of Pt in the oxidic state, which is around 11568 eV (obtained for non

reduced PtO_2/Al_2O_3-Cl reference). The Pt metal spectrum also shows two bands at 11580 and 11595 eV immediately after the whiteline region, while the spectrum of the oxidic form shows a characteristic dip after the whiteline and a fine structure near 11580 and 11593 eV. These observations are in very good agreement with those of Alayon *et al.*[viii]. The reduced monometallic Pt/Al_2O_3-Cl catalyst exhibits a XANES spectrum almost identical to that of the Pt foil, with identical whiteline intensity. This indicates that most of Pt is reduced to the metal state at 500°C. Compared with the oxidic sample, the edge energy (E_0) is shifted to lower energies, precisely to 11566.5 eV. Singh *et al.*[ix] reported an E_0 value of 11565.6 eV for bare Pt particles. A 0.4 eV shift was observed upon hydrogen absorption and it was suggested that the Fermi level had been pushed up by 0.4 eV. The 11566.5 eV whiteline position value reported in this work for reduced Pt/Al_2O_3-Cl is thus a little higher (by 0.5 eV), probably because of differences in loadings and preparation methods (presence of Cl in our samples) or due to slight differences in monochromator calibration or vacuum levels in the analytical cells. The features at 11573 eV, 11581 eV and 11595 eV attributed in the literature to multiple scattering of the photoelectron against neighbouring Pt atoms[71] are of very low intensity, indicating small platinum particles. This is consistent with STEM results showing average particle size of about 1.0 nm on this catalyst, which is in excellent agreement with reported results on reduced Pt/Al_2O_3-Cl with 0.9 nm particles.[viii]

3. DFT investigation of the structure of Pt_xSn_{13-x} clusters in the gas phase: simulated annealing

Mono- and bimetallic thirteen atoms clusters (Pt_xSn_{13-x}, with x = 13, 7 and 0) were modelled by DFT calculations. Isolated Pt_xSn_{13-x} clusters were optimized in a 20x20x20 $Å^3$ cubic cell, and the corresponding Brillouin-zone k-point mesh sampling was restricted to the gamma point. In the same spirit as our previous work on monometallic clusters,[x] a simulated annealing method was applied to find the most stable Pt_xSn_{13-x} clusters by scanning a large structural configuration space. This simulated annealing method is based on first-principles NVT velocity scaled molecular dynamics followed by quenches at 0 K.[xi]

The whole simulation time was at least 20 ps and the time for each step was set to 10 fs. The simulation temperature was adjusted for each cluster composition. 400 K was found as the most appropriate to find stable structures, starting from an arbitrary geometry consisting in a Pt cuboctahedron or biplanar structure, in which 0, 6 or 13 atoms of Pt were substituted by Sn.

Figure S3 depicts the evolution of the electronic potential energy for the Sn_{13} cluster during molecular dynamics runs performed at various temperatures, starting from a biplanar structure. More stable systems are found from the simulation performed at 400 K.

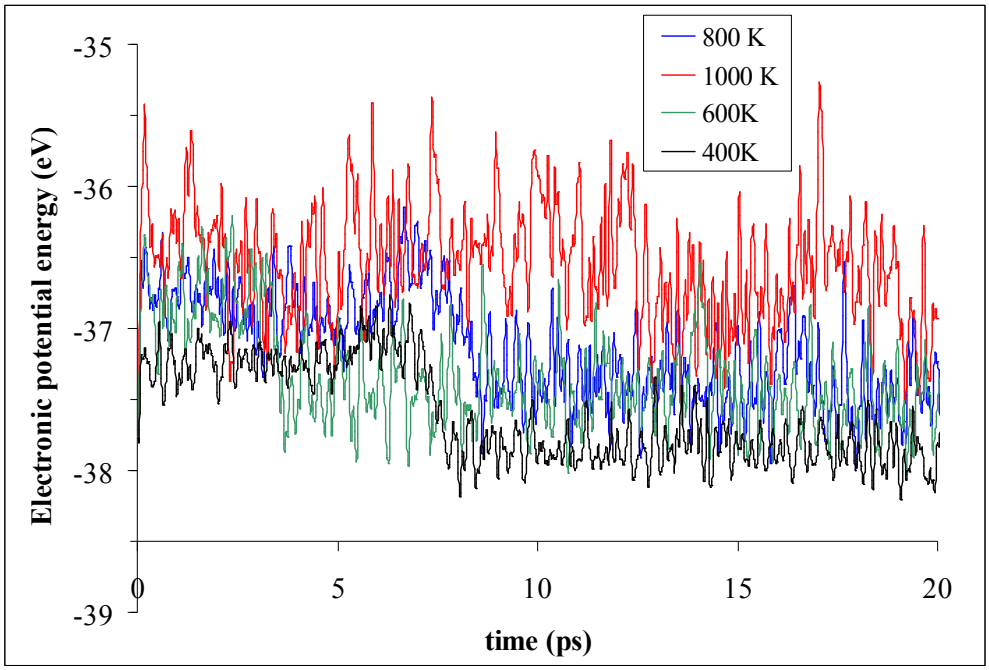

Figure S3. Evolution of the electronic potential energy of a Sn_{13} cluster as a function of the simulation time, for molecular dynamics run performed at various temperatures.

4. DFT investigation of the structure of Pt_xSn_{13-x} clusters supported on the γ-Al_2O_3 (100) surface

Clusters supported on γ-Al_2O_3 were modelled according to a method derived from ref.[xii], where the dehydrated (100) surface of gamma-alumina was shown to induce the stronger metal/support interaction for such cluster sizes. The γ-Al_2O_3(100) surface model is inherited from ref. [xiii;xiv] and is shown in Figure S4-a. Periodic slabs consist of four alumina layers separated by a vacuum thickness corresponding to more than two equivalent empty layers. Two alumina layers were fixed whereas the two other ones were relaxed.

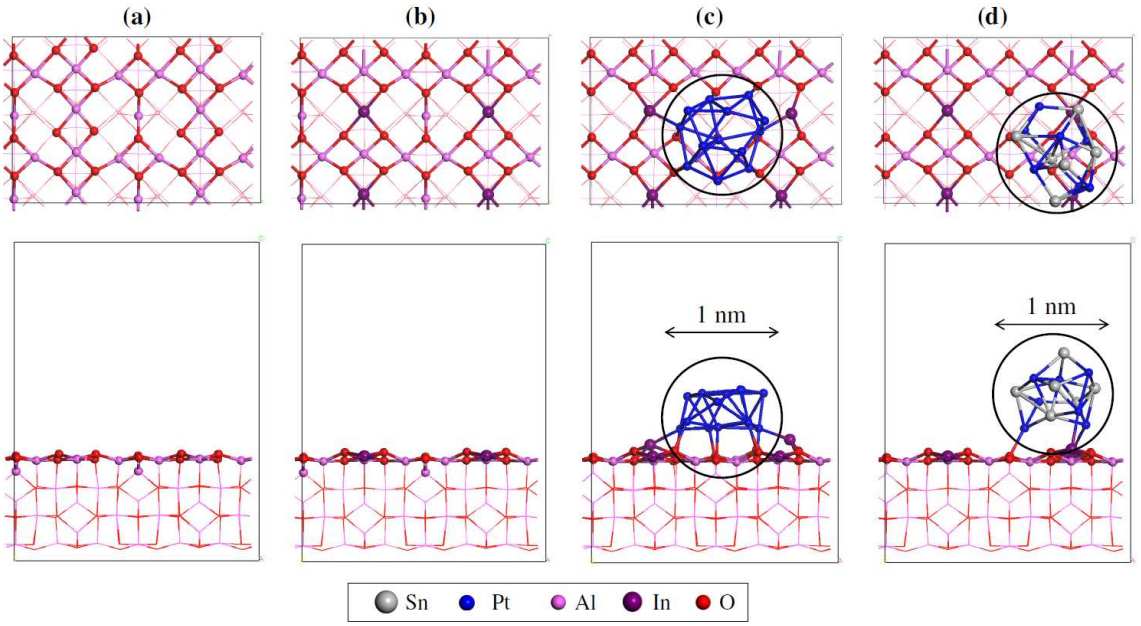

Figure S4. Top and side views and of typical unit cells modelled in the present work. (a) γ-Al_2O_3(100) slab. (b) γ-Al_2O_3(100) slab doped with four In atoms per unit cell. (c) Pt_{13}/γ-Al_2O_3(100) doped with In. The black circle depicts the diameter of a 1 nm particle.

The promotion of the γ-Al_2O_3(100) surface model by In^{3+} atoms was then studied by substitution of some Al^{3+} ions by In^{3+} species. The most stable substitution site is depicted in Figure S4-b. A dipolar correction following the axis perpendicular to the ionic surface was applied due to the introduction of In^{3+} ions on one side of the slab only.

Pt_xSn_{13-x} clusters were adsorbed and relaxed. Figures S4-c and d depict the examples of the Pt_{13} and the Pt_7Sn_6 clusters respectively.

We found that the most stable Pt_xSn_{13-x} / γ-Al_2O_3 system does not necessarily inherit from the gas phase morphology. In particular, stabilization of the system is reached by flattening of Pt_{13} into a biplanar structure. For the supported Pt_7Sn_6 system, we also found a Pt_7Sn_6 structure more stable than the gas phase cluster. Among numerous simulated Pt_7Sn_6 / γ-Al_2O_3 structures (including the deposition of the gas phase cluster), the best one was obtained from the previous Pt_{13} / γ-Al_2O_3 system where six Pt atoms were substituted by tin atoms.

A 1 nm diameter sphere is also depicted. Taking into account metallic radii of Pt and Sn atoms (1.39 and 1.63 Å to be added to the diameter of the simulated particle), it can be concluded that Pt_xSn_{13-x} can be considered as appropriate estimations of 1 nm particles.

5. Assignment of Mössbauer spectroscopy spectra

The following classification of Sn species was used in the paper.[xv]

1) Three types of Sn^{IV} oxides with isomer shifts δ ($mm.s^{-1}$) close to that of bulk SnO_2, that is $0.1<\delta<0.4$. These oxides are however distinguishable by their quadrupole splitting value Δ ($mm.s^{-1}$). The first oxide, labelled hereafter "SnO_2 0" corresponds to small, rather isolated, molecule like Sn particles which are not embedded in a surrounding matrix, but rather correspond to an octahedral SnO_6 cluster on the outermost sphere of a particle. Due to weak interaction with surrounding atoms, the Sn-O bonds are free of strain and relax to form a perfect octahedron, as reflected by the zero quadrupole splitting. The second oxide labelled "SnO_2 1" with $0.4<\delta<0.8$ $mm.s^{-1}$ forms a SnO_2-like lattice with Sn-O-Sn bridges, while the third with $0.8<\delta<1.5$ $mm.s^{-1}$(labelled Sn^{IV} 2) corresponds to a bimetallic lattice with Sn-O-Al or Sn-O-Pt bridges (eventually Sn-O-In), which is reflected in its relatively higher quadrupole splitting.

2) Three types of Sn^{II} oxides with characteristic δ and Δ values. The first oxide labelled "Sn^{II} 1" with Δ close to 1.3 $mm.s^{-1}$ and $2.55<\delta<2.65$ $mm.s^{-1}$ signifies an SnO-like structure. The second, labelled "Sn^{II} 2a" with $2.80<\delta<3.50$ $mm.s^{-1}$ and $\Delta>2.0$ $mm.s^{-1}$, signifies a Sn^{II} oxide with Sn in contact with another metal such as Pt or Al (eventually In). The last oxide labelled "Sn^{II} 2b" with $3.10<\delta<4.00$ $mm.s^{-1}$ and $0.9<\Delta<1.7$ $mm.s^{-1}$ is interpreted as a Sn^{II} oxide with Sn-O-Sn bridges.

3) Three categories of Sn^0 discriminated by their isomer shift and quadrupole splitting. The first type is Sn^0 present in $PtSn_x$ alloys with zero quadrupole splitting Δ and an isomer

shift δ which has been shown to linearly depend on (*x*).[xvi] Their isomer shifts could be thus used as a measure of the Pt:Sn atomic ratio. In this way, a phase with $1.4<\delta<1.7$ mm.s^{-1} signifies a Pt-rich $PtSn_x$ alloy, a $1.8<\delta<2.0$ mm.s^{-1} stands for almost equal Pt and Sn proportions and a $2.3<\delta<2.5$ mm.s^{-1} indicates a Sn-rich $PtSn_x$ alloy. The second category is a Sn phase present in Pt-Sn intermetallic particles with $1.25<\delta<2.15$ mm.s^{-1} and a non-zero quadrupole splitting. This phase is attributed to an oxo-metallic $Pt_xSn(O)$ species, with oxygen atoms creating a certain asymmetry in Sn environment, thus justifying the non-zero Δ value [vi]. The third type is non-alloyed Sn^0, presenting a majority of Sn-Sn bonds, with $2.20<\delta<2.50$ mm.s^{-1} and a $\Delta>0.6$ mm.s^{-1}. This phase was thus assigned to a solid solution where Sn is in contact with Al and Pt atoms that initially catalyzed its reduction into the metallic state.

Margitfalvi *et al* [xvii,xviii,xix] described two types of Pt-Sn alloys, the first lying in the 1.20-1.56 mm.s^{-1} isomer shift range and the second in the 2.23-2.35 mm.s^{-1} isomer shift range. The former was assigned to Sn dissolved in Pt (Sn < 6 at.%) and/or to Pt_3Sn. The latter, with higher isomer shifts, was attributed to Sn rich Pt_2Sn_3 and $PtSn_4$ phases. Charlton *et al.* [vii] reported a study on the dependence of the isomer shift of PtSn alloys on their Sn atomic content. It was found that the Sn isomer shift in these alloys could be linearly traced as a function of Sn atomic concentration in the alloy, and that there was a gradual decrease of δ values of Sn solid solutions in Pt relative to the Pt_3Sn alloy (as a function of Sn atomic concentration). We tend therefore to consider the intermetallic phases observed below $\delta = 1.20$ mm.s^{-1} (with $\Delta>0$) equally as substitutional alloys, in which Sn atoms are also anchored to O or even Cl atoms, which creates non-zero quadrupole splitting values. The decrease of the quadrupole splitting of the observed $Pt_xSn(O)$ phase is therefore indicative of the impact of the In-alumina interactions on the structure of the later formed Pt-Sn nano-clusters.

References

[i] Mojet, B. L.; Miller, J. T.; Ramaker, D. E.; Koningsberger, D. C. *J. Catal.* **1999**, *186*, 373-386.

[ii] Oudenhuijzen, M. K.; van Bokhoven, J. A.; Miller, J. T.; Ramaker, D. E.; Koningsberger, D. C. *J. Am. Chem. Soc.* **2005**, *127*, 1530-1540.

[iii] Ramaker, D. E.; Koningsberger, D. C. *Phys. Chem. Chem. Phys.* **2010**, *12*, 5514-5534.

[iv] Stakheev, A. Y.; Zhang, Y.; Ivanov, A. V.; Baeva, G. N.; Ramaker, D. E.; Koningsberger, D. C. *J. Phys. Chem. C* **2007**, *111*, 3938-3948.

[v] Lytle, F. W. *J. Catal.* **1976**, *43*, 376-379.

[vi] Mansour, A. N.; Cook, J. W.; Sayers, D. E. *J. Phys. Chem.* **1984**, *88*, 2330-2334.

[vii] van Bokhoven, J. A.; Miller, J. T. *J. Phys. Chem. C* **2007**, *111*, 9245-9249.

[viii] Alayon, E. M. C.; Singh, J.; Nachtegaal, M.; Harfouche, M.; van Bokhoven, J. A. *J. Catal.* **2009**, *263*, 228-238.

[ix] Singh, J.; Nelson, R. C.; Vicente, B. C.; Scott, S. L.; van Bokhoven, J. A. *Phys. Chem. Chem. Phys.* **2010**, *12*, 5668-5677.

[x] Hu C.H.;, Chizallet C.; Toulhoat H.; Raybaud P., *Phys. Rev. B* **2009**, *79*, 195416.

[xi] Jaswal S.S.; Hafner J., *Phys. Rev. B* **1988**, *38,* 7311-7319.

[xii] Hu C.H.; Chizallet C.; Mager-Maury C.; Corral Valero M.; Sautet P.; Toulhoat H.; Raybaud P., J. Catal. **2010**, *274,* 99-110.

[xiii] Digne M.; Sautet P.; Raybaud P.; Euzen P.; Toulhoat H. *J. Catal.* **2002**, *211*, 1-5.

[xiv] Digne M.; Sautet P.; Raybaud P.; Euzen P.; Toulhoat H. *J. Catal.* **2004**, *226* ,54-68.

[xv] Olivier-Fourcade J.; Womes M.; Jumas J.-C.; Le Peltier F.; Morin S.; Didillon B. *ChemPhys Chem* **2004**, *5,* 1734-1744.

[xvi] Charlton J. S.; Cordey-Hayes M.; Harris I. R. *J. Less-Common Metals* **1970**, *20*, 105-112.

[xvii] Margitfalvi J. L.; Borbáth I.; Lázár K.; Tfirst E.; Szegedi A.; Hegedűs M.; Gőbölös S. *J. Catal.* **2001**, *203,* 94-103.

[xviii] Margitfalvi J. L.; Borbáth I.; Hegedűs M.; Tfirst E.; Gőbölös S.; Lázár K. *J. Catal.* **2000**, *196*, 200-204.

[xix] Margitfalvi J. L.; Vankó Gy.; Borbáth I.; Tompos A.; Vértes A. *J. Catal.* **2000**, *190,* 474-477.